

RESEARCH ARTICLE

Tissue-Engineered Small Diameter Arterial Vascular Grafts from Cell-Free Nanofiber PCL/Chitosan Scaffolds in a Sheep Model

Takuma Fukunishi¹, Cameron A. Best², Tadahisa Sugiura², Toshihiro Shoji², Tai Yi², Brooks Udelsman³, Devan Ohst⁴, Chin Siang Ong¹, Huaitao Zhang¹, Toshiharu Shinoka², Christopher K. Breuer², Jed Johnson⁴, Narutoshi Hibino^{1*}

1 Department of Cardiac Surgery, Johns Hopkins University, Baltimore, MD, United States of America, **2** Tissue Engineering and Center for Cardiovascular and Pulmonary Research, Nationwide Children's Hospital, Columbus, OH, United States of America, **3** Yale University School of Medicine, New Haven, CT, United States of America, **4** Nanofiber Solutions Inc, Columbus, OH, United States of America

* nhibino1@jhmi.edu



OPEN ACCESS

Citation: Fukunishi T, Best CA, Sugiura T, Shoji T, Yi T, Udelsman B, et al. (2016) Tissue-Engineered Small Diameter Arterial Vascular Grafts from Cell-Free Nanofiber PCL/Chitosan Scaffolds in a Sheep Model. PLoS ONE 11(7): e0158555. doi:10.1371/journal.pone.0158555

Editor: John S Forsythe, Monash University, AUSTRALIA

Received: February 28, 2016

Accepted: June 19, 2016

Published: July 28, 2016

Copyright: © 2016 Fukunishi et al. This is an open access article distributed under the terms of the [Creative Commons Attribution License](https://creativecommons.org/licenses/by/4.0/), which permits unrestricted use, distribution, and reproduction in any medium, provided the original author and source are credited.

Data Availability Statement: All relevant data are within the paper.

Funding: This study was supported by grants from the NIH Center for Accelerated Innovations: Technology Development Program (1UH54HL119810-01) to NH and JJ. C. Breuer and T. Shinoka received grant support from Gunze Ltd (Kyoto, Japan). Nanofiber solutions provided support in the form of materials and salaries to DO and JJ. The specific roles of these authors are articulated in the 'author contributions' section.

Abstract

Tissue engineered vascular grafts (TEVGs) have the potential to overcome the issues faced by existing small diameter prosthetic grafts by providing a biodegradable scaffold where the patient's own cells can engraft and form functional neotissue. However, applying classical approaches to create arterial TEVGs using slow degrading materials with supra-physiological mechanical properties, typically results in limited host cell infiltration, poor remodeling, stenosis, and calcification. The purpose of this study is to evaluate the feasibility of novel small diameter arterial TEVGs created using fast degrading material. A 1.0mm and 5.0mm diameter TEVGs were fabricated with electrospun polycaprolactone (PCL) and chitosan (CS) blend nanofibers. The 1.0mm TEVGs were implanted in mice ($n = 3$) as an unseeded infrarenal abdominal aorta interposition conduit., The 5.0mm TEVGs were implanted in sheep ($n = 6$) as an unseeded carotid artery (CA) interposition conduit. Mice were followed with ultrasound and sacrificed at 6 months. All 1.0mm TEVGs remained patent without evidence of thrombosis or aneurysm formation. Based on small animal outcomes, sheep were followed with ultrasound and sacrificed at 6 months for histological and mechanical analysis. There was no aneurysm formation or calcification in the TEVGs. 4 out of 6 grafts (67%) were patent. After 6 months *in vivo*, $9.1 \pm 5.4\%$ remained of the original scaffold. Histological analysis of patent grafts demonstrated deposition of extracellular matrix constituents including elastin and collagen production, as well as endothelialization and organized contractile smooth muscle cells, similar to that of native CA. The mechanical properties of TEVGs were comparable to native CA. There was a significant positive correlation between TEVG wall thickness and CD68⁺ macrophage infiltration into the scaffold ($R^2 = 0.95$, $p = 0.001$). The fast degradation of CS in our novel TEVG promoted excellent cellular infiltration and neotissue formation without calcification or aneurysm. Modulating host macrophage infiltration into the scaffold is a key to reducing excessive neotissue formation and stenosis.

Competing Interests: This study was supported by electrospun nanofiber PCL/CS Tissue Engineered Vascular Grafts from Nanofiber Solution Inc. Nanofiber solutions has no patents to declare. C. Breuer and T. Shinoka received grant support from Gunze Ltd (Kyoto, Japan). This does not alter the authors' adherence to the PLOS ONE policies on sharing materials and data.

Introduction

Coronary artery disease (CAD) and peripheral vascular disease (PVD) are leading causes of death and impaired quality of life. Vascular graft transplantations, such as coronary artery bypass grafts (CABG) and distal limb bypass [1], are common operations performed in approximately 600,000 patients annually in the USA [2]. The autologous great saphenous vein and internal mammary artery are small diameter grafts (<6mm) widely accepted as the current gold standard for CABG surgery. These autografts have several disadvantages in patients such as inherent size mismatches, pre-existing vascular disease (such as atherosclerosis), and supply shortage due to previous procedures. Expanded polytetrafluoroethylene (ePTFE, Gore-Tex[®]) is the most commonly used synthetic graft material for distal limb bypass, and has been clinically successful in situations where the graft diameter is larger than 6mm (high flow, low resistance circulation) [3–5]. However, its efficacy is limited in small diameter vascular grafts (<6mm) due to thrombosis (platelet adhesion and aggregation), progressive stenosis (neointimal hyperplasia and over-proliferation of smooth muscle cells), calcium deposition, host rejection, increased risk of infection and the need for anticoagulation therapy [6–12].

Small diameter tissue engineered vascular grafts (TEVGs) have been developed to withstand the high pressures of the arterial circulation. In order to create functional compliance, the formation of well-organized vascular neotissue through the vascular remodeling process is paramount.[13–16]. Therefore, an ideal graft will undergo rapid vascular remodeling by facilitating cellular infiltration and scaffold degradation. Recently, three-dimensional porous nanofiber scaffolds fabricated by electrospinning have been widely investigated as arterial TEVGs [17, 18]. Previous studies demonstrated that slow degrading polycaprolactone (PCL) or polylactic acid (PLA) can provide adequate mechanical properties as small diameter TEVGs when applied to the abdominal aorta in the mouse and rat models. However, slow degrading PCL grafts had limited cell infiltration, poor neotissue formation, and localized calcification in the long-term [13, 19, 20].

Recent studies have investigated materials fabricated by combining both synthetic polymers and natural proteins, such as collagen, elastin, gelatin, chitosan (CS). These hybrid scaffold materials have promising potential for the next generation of small diameter arterial TEVGs [21–24] because of their fast degradation and hydrophilic characteristics that promote better cell infiltration, proliferation and neotissue formation. CS and synthetic polymer combinations have been successfully used as tissue engineering scaffolds for bone, cartilage and skin, but little is known about their potential for tissue engineered vascular grafts, especially in large animal models [17, 18, 25].

The purpose of this study is to investigate the feasibility of unseeded (cell-free) small diameter hybrid TEVGs (5mm) fabricated by electrospinning a blend of synthetic PCL and natural CS in small and large animal models of high pressure circulation over a 6 month time course.

Materials and Methods

Study design

We evaluated the efficacy of a novel cell-free nanofiber PCL/chitosan TEVGs as arterial conduits implanted in mice at the end of 6 months. The TEVGs were implanted into mice (n = 3) as an infrarenal abdominal aorta (IAA) interposition grafts and all demonstrated patency without graft narrowing or rupture (100%). We subsequently implanted the TEVGs in sheep (n = 6) as carotid artery (CA) interposition grafts. The TEVGs were explanted at 6 months post-implantation for evaluation of neotissue formation, biocompatibility and mechanical

properties. There were no instances of data exclusion in this study and outliers were also included in the data analysis.

Scaffold fabrication

Polycaprolactone (PCL) (Mn 70,000–90,000) and chitosan (CS) (Medium molecular weight) were purchased from Sigma Aldrich Co, LLC (Missouri, USA). Hexafluoroisopropanol (HFIP) and acetic acid (AA) (99.7%) were purchased from Oakwood Chemicals and Sigma Aldrich, respectively. All polymers and solvents were used without further modification.

Chitosan (CS) was dissolved in a 9:1 w/w solution of hexafluoroisopropanol (HFIP) and acetic acid to produce a 0.15 wt% CS solution and was stirred via a magnetic stir bar for 3 hours at 50°C. Polycaprolactone (PCL) was then added to the CS solution in a 20:1 w/w ratio of PCL and CS and stirred via a magnetic stir bar for 21 hours at 50°C. The PCL/CS solution was placed in a 20cc luer-lok syringe and dispensed at a flow rate of 5ml/h through a 20 gauge blunt needle tip. A 1.0mm diameter mandrel was used for the mouse grafts while a 5.0mm diameter mandrel was used for the ovine grafts. The mandrel was positioned 20cm from the needle tip and was rotated at 100 RPM. A +25kV charge was applied to the needle tip and a -4kV charge was applied to the mandrel. The electrospun nanofibers were deposited to create a $100 \pm 10\mu\text{m}$ wall thickness tube for the murine grafts and $400 \pm 40\mu\text{m}$ wall thickness tube for the ovine grafts. The PCL/CS tubes were cut into 0.3cm lengths for the murine grafts and 1.5cm lengths for the ovine grafts. Finally, all the PCL/CS TEVGs were terminally sterilized with 50kGy of gamma irradiation.

Mechanical testing

Compliance and burst pressure data were acquired as previously described [26]. In brief, data was acquired using an MTS Systems Corporation (Minnesota, USA) load frame fitted with a 50 lb load cell with a force resolution of 10^{-4} pounds and a linear displacement resolution of 10^{-8} inches. Compliance testing was performed using a displacement velocity of 1.5 mm per minute and acquisition rate of 4 data points per second utilizing Laplace's Law [27, 28] to correlate linear force and displacement to compliance. Burst pressure testing was performed using a displacement velocity of 50 mm per minute and acquisition rate of 4 data points per second utilizing Laplace's Law [28, 29] to correlate linear force and displacement to burst pressure.

Samples were placed around two parallel L-shaped steel rods, one rod was attached to the base of the universal testing machine and the other to the load cell. The samples were strained perpendicular to the length of the sample. Compliance was calculated using systolic and diastolic pressures of 120 mmHg and 80 mmHg, respectively. Burst pressure was calculated using the maximum force before failure.

Degradation rate *in vitro*

ASTM D638 Type V tensile dogbones were cut from sheets of the PCL/CS nanofiber and placed in Ringers solution and incubated at 37°C to mimic *in vivo* hydrolytic degradation conditions. Mass and mechanical properties were measured at 1, 2, 3 and 4 weeks to determine the degradation profile of this nanofiber composite material. Mass loss was determined by drying each sample under vacuum for 72 hours before weighing. Tensile testing was performed on an MTS Systems Corporation (Minnesota, USA) load frame with a 10N load cell and an elongation rate of 15mm/min. 5 samples were used for each test at each time point.

Graft implantation

All mice procedures received prior approval from the institutional animal care and use committee at Yale University. Nanofiber-PCL/CS TEVGs were implanted as interpositional grafts in the infrarenal abdominal aorta (IAA) in 3 female CB-17 severe combined immunodeficient-beige (SCID/bg) mice ($n = 3$). Implantation was accomplished using a sterile microsurgical technique described previously[30]. Briefly, anesthetized mice were placed in the supine position and opened with an abdominal midline incision. A portion of the infrarenal abdominal aorta was exposed, cross-clamped, and excised. Three-millimeter length scaffolds were then inserted as interposition grafts using a running 10-0 nylon suture for the end-to-end proximal and distal anastomoses. TEVG patency, wall thickness, and lumen diameter were assessed *in vivo* using high frequency ultrasound system (Vevo 770, Visualsonics, Toronto, Canada) with a RMV-704 transducer until the 6 months end point.

The animal care and use committee at the Q-Test Laboratories (Columbus, Ohio) approved the care, use, and monitoring of animals for sheep experiments. Nanofiber-PCL/CS TEVGs were implanted as right carotid artery interposition grafts in sheep ($n = 6$, body weight: 23.9 ± 5.0 kg). All sheep were anesthetized with 1.5% isoflurane during surgery. The carotid artery was exposed and heparin (100 IU/kg) was administered intravenously. The TEVG was implanted as a carotid artery interposition graft using standard running 7-0 prolene suture (Ethicon Inc.). Hemostasis was obtained, and the muscle, subcutaneous tissue, and dermal incision layers were closed. Antibiotic treatment (cefazolin) was administered intra-operatively and 7 days post-operatively. All sheep were maintained on a daily oral medication of aspirin (325 mg/day) until the 6 months end point. Color Doppler ultrasound was performed at 1, 3 and 6 months to determine graft patency and lumen diameter. Animals were euthanized using pentobarbital sodium, and grafts were explanted at 6 months after surgery.

Histology and immunohistochemistry

Explanted TEVG samples were fixed in 10% formalin for 24 hours at 4°C, then embedded in paraffin. For standard histology, tissue sections were stained with hematoxylin and eosin (H&E), Masson's trichrome, picosirius red, Hart's, and von Kossa. For immunohistochemistry, tissue sections were deparaffinized, rehydrated, and blocked for endogenous peroxidase activity and nonspecific staining. The primary antibodies used included: von Willebrand Factor (vWF, Dako, 1:2000), α -smooth muscle actin (SMA, Dako, 1:500), calponin (Abcam, 1:500), myosin heavy chain (MHC, Abcam, 1:500), CD68 (Abcam, 1:200). Antibody binding was detected using biotinylated secondary antibodies, followed by incubation with streptavidinated HRP. Color development was performed by chromogenic reaction with 3,3'-diaminobenzidine (Vector). Nuclei were counterstained with hematoxylin (Gill's formula, Vector).

Histological and quantitative analysis

The lumen diameter, wall thickness, remaining scaffold area, and collagen quantitative analyses were measured from H&E and picosirius red staining using Image J software (Image Processing and Analysis in Java; National Institutes of Health, Bethesda, MD, USA). Macrophages, identified by positive CD68 expression, were quantified for each explanted scaffold. Four sections of each individual sample were counted at 40x (high powered field; HPF) and averaged for a total of six samples.

Statistical analysis

For all experiments, data are represented as mean \pm SEM, and statistically significant differences between groups were determined using Student's t-test and Pearson correlation test. A paired t-test was performed comparing native tissue to tissue-engineered samples. A *p*-value less than 0.05 was considered statistically significant. Statistical analysis was performed using Graphpad Prism (GraphPad Software, Inc., version 6, CA, USA).

Results

Scaffold characterization

Scanning electron microscopy revealed very fine uniform fibers with a diameter of $150\text{nm} \pm 62\text{nm}$ (Fig 1A and 1B). The slow mandrel rotation speed allowed the scaffold to have no preferential alignment of fibers and isotropic properties. Additionally, the PCL and chitosan were blended within each fiber, rather than a scaffold comprised of monolithic PCL fibers and monolithic chitosan fibers (Fig 1C). *In vitro* characterization of PCL/CS scaffold degradation through 4 weeks demonstrated an approximately 50% loss in ultimate tensile strength (UTS) by 2 weeks with a similar decrease in strain at failure that was followed by a plateauing out to 4 weeks (Fig 1E and 1F). In contrast, mass remained constant throughout the experimental time course (Fig 1D).

Nanofiber PCL/chitosan TEVGs in a mouse model

Cell-free nanofiber PCL/CS scaffolds were successfully implanted as interpositional IAA grafts and all mice survived until the 6 months end point without complications. All TEVGs remained patent without evidence of thrombosis or aneurysm formation despite initial graft oversizing of 50% (Fig 2A). With regards to lumen diameter and wall thickness, Doppler

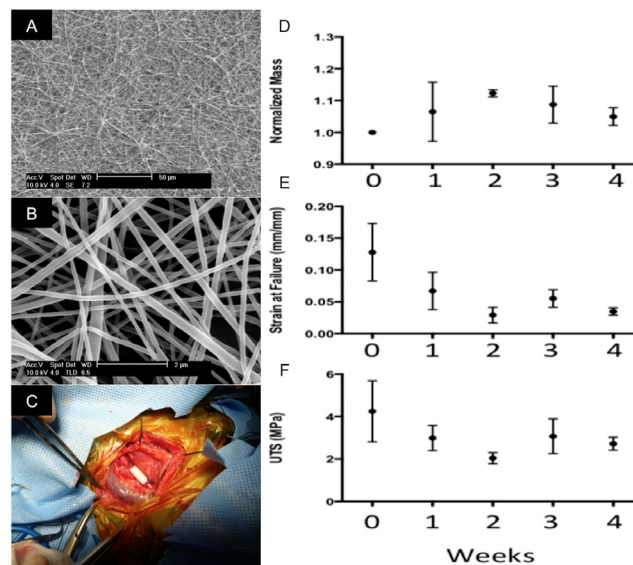


Fig 1. Characterization of Scaffolds. Representative scanning electron microscopy of PCL/CS TEVGs prior to implantation at low powered (A) and high powered fields (B). Perioperative image of freshly implanted scaffold (C). *In vitro* degradation of PCL/CS measured by change in mass (D), change in strain at failure (E) and change in UTS (F) (n = 5).

doi:10.1371/journal.pone.0158555.g001

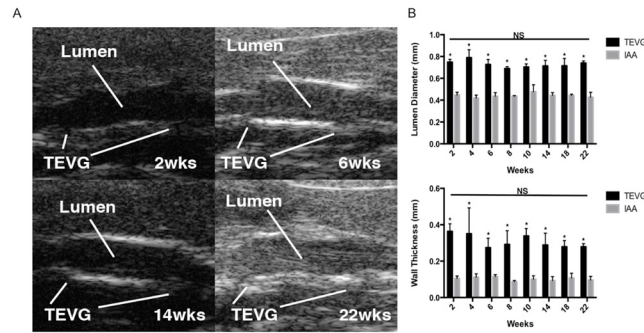


Fig 2. Preliminary study results. Representative Doppler ultrasound images of TEVGs at various time points showing graft patency *in vivo* (A). TEVG lumen diameter and wall thickness as measured by Doppler ultrasound (n = 3). Data in graphs are expressed as mean ± SD. *P < 0.05. There was a statistically significant difference in both luminal diameter and wall thickness between TEVG and IAA at each time point. However, no statistically significant difference (NS) was found between all time points for either TEVG or native IAA (B).

doi:10.1371/journal.pone.0158555.g002

ultrasound revealed no evidence of graft failure, and no statistically significant differences were found between time points for both the TEVG or native IAA (Fig 2B).

Nanofiber PCL/chitosan TEVGs in a sheep model

Mechanical properties. Compared the native CA, the burst pressure of the graft pre-operation was significantly less (Fig 3A, $1.46 \pm 0.52\text{MPa}$ vs. $0.39 \pm 0.08\text{MPa}$, $p = 0.0371$). There was also a statistically significant difference in burst pressure between the TEVG at 6 months and graft pre-operation (Fig 3A, $1.37 \pm 0.36\text{MPa}$ vs. $0.39 \pm 0.08\text{MPa}$, $p = 0.0224$). However, there was no significant difference in burst pressure between the native CA and TEVG at 6 months (Fig 3A, $1.46 \pm 0.52\text{MPa}$ vs. $1.37 \pm 0.36\text{MPa}$, $p = 0.4059$). With regards to compliance, there was no significant difference between the native CA and graft pre-operation (Fig 3B, $11.98 \pm 2.02\%$ vs. $14.04 \pm 1.50\%$, $p = 0.1115$). However, the TEVG at 6 months was significantly less compliant when compared to the native CA (Fig 3B, $6.58 \pm 1.76\%$ vs. $11.98 \pm 2.02\%$, $p = 0.0125$) and graft pre-operation (Fig 3B, $6.58 \pm 1.76\%$ vs. $14.04 \pm 1.50\%$, $p = 0.0018$).

Histological results. H&E staining showed that cellular infiltration was extensive in the TEVG and therefore the pore size/fiber diameter of the scaffold was enough to allow for cell infiltration (Fig 4A and 4E), and a patency rate of 66.7% (4/6) without any incidence of graft dilatation or rupture. The inner diameter of nanofiber TEVG and native CA measured $2.90 \pm 0.92\text{mm}$ and $2.25 \pm 0.16\text{mm}$ respectively (Fig 5A, $p = 0.3102$). Ultrasound measurements

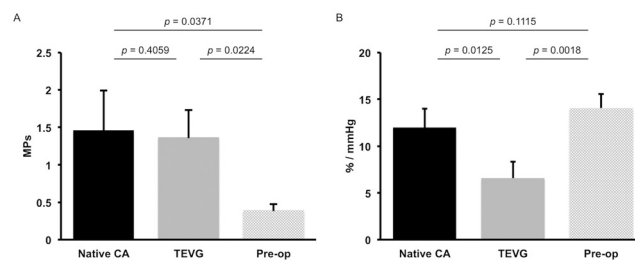


Fig 3. Mechanical properties. The burst pressure (A) and compliance (B) of the native CA, TEVG, and pre-operation/implantation were indicated respectively. There was no significant difference in burst pressure between the native CA and TEVG at 6 months. However, the TEVG at 6 months was significantly less compliant when compared to the native CA.

doi:10.1371/journal.pone.0158555.g003

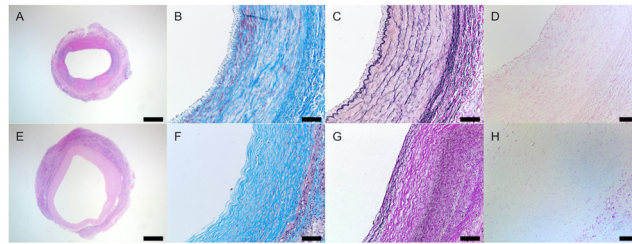


Fig 4. Histological assessment of vascular neotissue formation at 6 months. The vascular neotissue including collagen and elastin deposition is similar to native carotid artery (CA) without ectopic calcification. Representative pictures are shown for H&E staining (A, E), Masson's trichrome staining (B, F), Hart's staining (C, G), and von Kossa staining (D, H). Native CA (A-D) is compared to nanofiber PCL/CS TEVGs (E-H). The scale bar represents a length of 1,000µm for A and E, and 100µm otherwise.

doi:10.1371/journal.pone.0158555.g004

revealed no significant difference between the TEVG and native CA diameter at 3 and 6 months, as the TEVG gradually remodeled to mimic the CA lumen in size (Fig 6). However, there was a statistically significant difference in wall thickness between the TEVG and native CA (Fig 5B, TEVG: 1.18 ± 0.08mm vs. native CA: 0.75 ± 0.07mm, $p = 0.0102$).

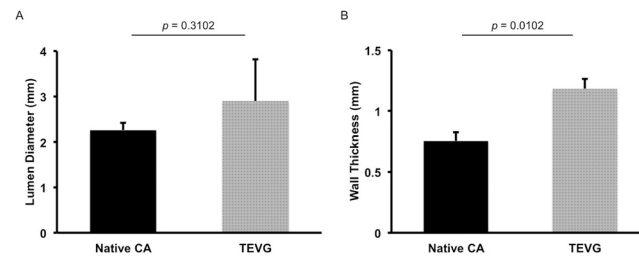


Fig 5. Lumen diameter and wall thickness analysis. Histomorphometric comparison of the inner diameter (A) and wall thickness (B) between the nanofiber PCL/CS TEVGs and the native CA revealed no significant difference in the inner diameter and a significant difference in the wall thickness.

doi:10.1371/journal.pone.0158555.g005

	1M	3M	6M
Native CA (mm)	3.18 ± 0.20	3.36 ± 0.76	3.20 ± 0.75
TEVG (mm)	4.41 ± 0.18	3.55 ± 0.65	3.22 ± 0.96
p - value	0.0004	0.0079	0.8629

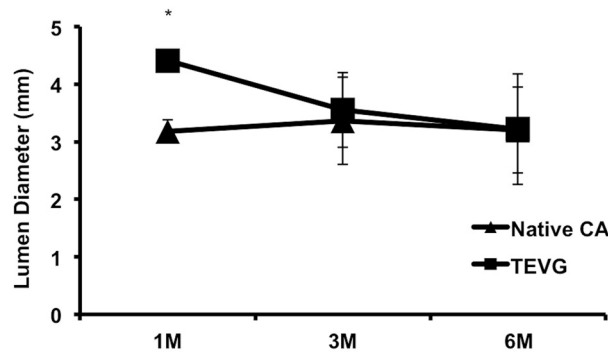


Fig 6. Inner diameter over time by serial ultrasound. Comparison between the TEVG and native carotid artery (CA) in patent TEVGs revealed that the TEVG lumen diameter gradually mimics the native CA. There was a statistically significant difference at 1 month, but no significant differences at 3 and 6 months after implantation. The symbol (*) denotes statistical significant differences between the native CA and TEVG at 1 month.

doi:10.1371/journal.pone.0158555.g006

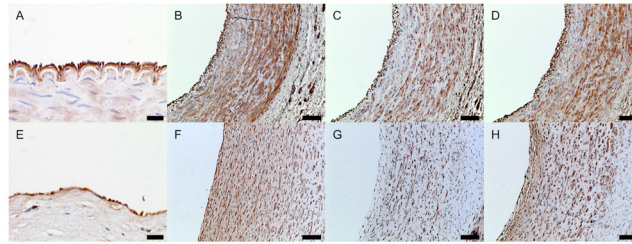


Fig 7. Endothelialization and smooth muscle cell (SMC) differentiation in TEVG neotissue at 6 months. TEVG ECs and SMCs were mature and well-organized, which reflected the native carotid artery (CA) in area, distribution, and density. Representative photomicrographs are shown for vWF (A, E), α -smooth muscle actin (SMA) (B, F), calponin (C, G), and myosin heavy chain (MHC) (D, H) for native CA (A-D) and nanofiber PCL/CS TEVGs (E-H). The scale bar represents a length of 20 μ m for A and E, and 100 μ m otherwise.

doi:10.1371/journal.pone.0158555.g007

On the graft lumen surface, a cellular monolayer stained positively for vWF, indicating endothelial cell layer formation (Fig 7A and 7E). The luminal surfaces of patent grafts displayed no evidence of microthrombosis.

Histological assessment of extracellular matrix (ECM) constituents, including collagen and elastin, was similar to native CA. Collagen synthesis was confirmed with collagen type I and III expression. The ECM (Fig 4B and 4F), collagen deposition and density in the TEVG resembled that of native tissue. Picosirius red staining revealed red, green, and yellow/orange fibers (Fig 8A and 8B). Red fibers were indicative of mature collagen type I fibers, whereas green fibers represented immature collagen type III fibers. Yellow/orange (intermediate between red and green) fibers characterized tissue growth and maturation representing

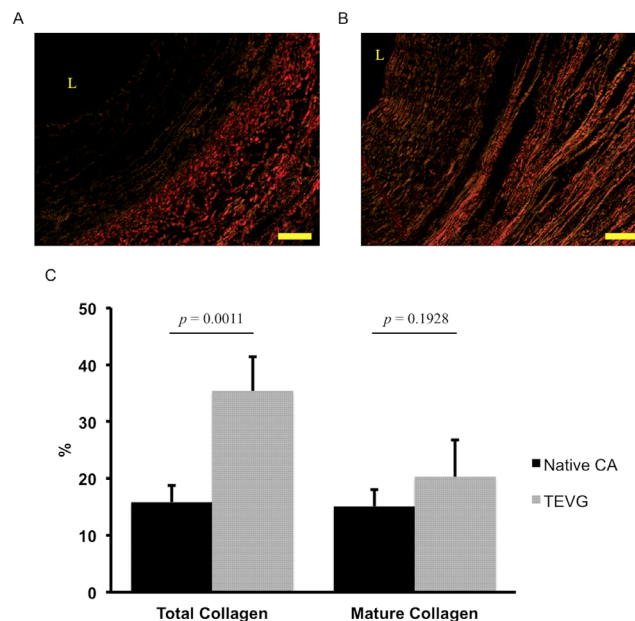


Fig 8. Collagen visualization and quantification. The collagen of native CA (A) and TEVG (B) were visualized by picosirius red staining using polarized light. In collagen analysis (C), there was significantly more total collagen volume in the TEVG when compared with native CA, whereas the volume of mature collagen was similar in both the TEVG and native CA. The scale bar is represents a length of 100 μ m for A and B. The symbol (L) denotes the vessel lumen.

doi:10.1371/journal.pone.0158555.g008

a spectrum consisting of collagen type III (immature) to type I (mature) and provided neovessel biomechanical properties as needed as the scaffold degrades. There was significantly more total collagen volume in the TEVG when compared with native CA (Fig 8C, $35.40 \pm 6.03\%$ vs. $15.82 \pm 2.92\%$, $p = 0.0011$), whereas the volume of mature collagen type I was similar in both the TEVG and native CA (Fig 8C, $20.30 \pm 6.47\%$ vs. $15.09 \pm 2.94\%$, $p = 0.1928$). However, the volume of intermediary type III to type I collagen was significantly larger in the TEVG when compared with native CA ($15.10 \pm 7.11\%$ vs. $0.73 \pm 0.23\%$, $p = 0.0068$). In addition, there was no evidence of the immature collagen in both the TEVG and native CA at 6 months. Hart's staining demonstrated that elastin was deposited within the internal and external elastic lamina of the TEVG, but it did not compare to the thickness and organization of elastin present in the native CA (Fig 4C and 4G). There was no evidence of ectopic calcification at 6 months (Fig 4D and 4H).

H&E staining observed with polarized light microscopy revealed that only $9.12 \pm 5.41\%$ of the nanofiber scaffold material remained at 6 months, and this material tended to remain between the outside of the neointima and neoadventitia.

Smooth muscle cell layer. We were successfully able to stain for multiple SMC phenotypes using α -SMA, calponin and MHC. Staining revealed that the organization and maturity of vascular SMCs in the TEVG were similar to that of native CA at 6 months. Contractile SMCs, identified by calponin and MHC positive staining, are characterized by elongated spindle-shaped cells. A multilayer of calponin and MHC positive cells was circumferentially organized and maintained adequate wall thickness from the subintimal to medial layers (Fig 7, native CA: C, D, TEVG: G, H). Synthetic SMCs, myofibroblasts, and many mesenchymal cell types are identified by α -SMA positive staining and show a cuboidal cobblestone-like morphology when compared to contractile SMCs. A multilayered population of α -SMA positive cells was primarily present in the neointima, suggesting that the TEVG may not have been a completely mature neo-artery at 6 months and active vascular remodeling was still occurring at this time point (Fig 7B and 7F). Alternatively, mature SMCs could also express α -SMA, and the α -SMA-positive staining observed may be due to mature SMCs in the TEVG.

Macrophage infiltration. CD68⁺ macrophages are a primary cell population in the inflammation-mediated process of vascular remodeling that occurs upon implantation of a resorbable scaffold. There was a statistically significant difference in macrophage infiltration (Fig 9A, patent group: $25.00 \pm 5.08/\text{HPF}$ vs. occluded group: $68.13 \pm 1.24/\text{HPF}$, $p = 0.0004$) and wall thickness (Fig 9B, patent group: $1.18 \pm 0.08\text{mm}$ vs. occluded group $1.90 \pm 0.20\text{mm}$, $p = 0.0025$) between patent and occluded TEVGs. Furthermore, we found a significant positive correlation between TEVG wall thickness and macrophage infiltration into the scaffold (Fig 9C, $R^2 = 0.9499$, $p = 0.0010$).

Discussion

The results of this study demonstrate the efficacy of a novel unseeded small-diameter arterial TEVG using electrospun PCL/CS nanofiber scaffolds in a sheep model of carotid artery interposition grafting. Serial ultrasound revealed that the initial difference between the TEVG and native CA diameters gradually resolved over the course of remodeling, and the lumen diameter of the TEVG matched that of the native CA after 3 months. The TEVG displayed an EC monolayer, contractile vascular SMCs, and ECM deposition, which all resembled the native CA. The mechanical profile of the TEVG 6 months after implantation also resembled that of the native CA. Based on these data, we suggest that the formation of well-organized vascular neotissue without aneurysm, graft rupture, or calcification at 6 months follow-up demonstrates that the TEVG underwent successful remodeling.

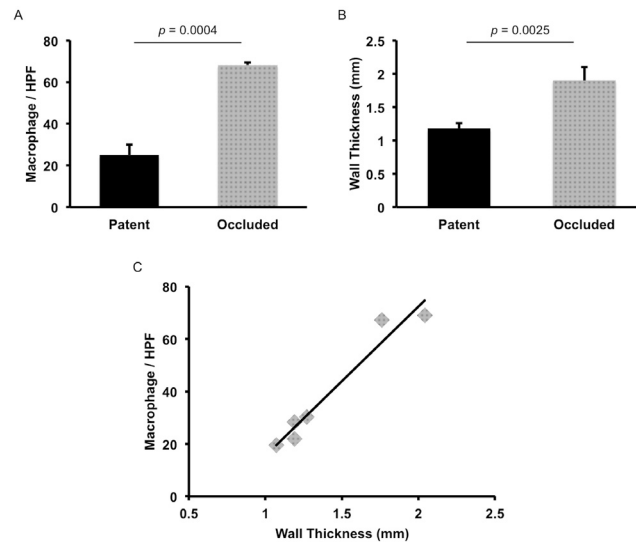


Fig 9. Macrophage analysis. The macrophage infiltration (A) and wall thickness (B) of patent TEVG were significantly less than that of occluded TEVGs. In addition, there was a significant positive correlation between the wall thickness of nanofiber PCL/CS TEVGs and CD68⁺ macrophages/HPF in the PCL/CS TEVGs (C).

doi:10.1371/journal.pone.0158555.g009

Electrospun PCL/CS nanofiber TEVGs have been investigated *in vitro* and *in vivo* due to their biocompatibility and favorable biomechanical properties. In 2005, an *in vitro* study investigating a hybrid PCL/CS material for tissue engineering applications demonstrated a significant improvement in mechanical properties, as well as support for cellular activity relative to PCL alone [31]. More recently, several reports have shown the effect of heparin coating or cell seeding of CS TEVGs [18, 25, 32], but there are currently no reports investigating the application of a CS TEVG *in vivo* without cell seeding or coating. Combining CS and PCL for TEVG scaffolds can provide faster degradation profiles than PCL alone due to the inherent properties of CS including its low molecular weight and its low degree of deacetylation [33]. Indeed, CS fibers are reported to have rapid *in vitro* degradation kinetics (~5 days), and degrade even faster *in vivo* [34]. Therefore, we hypothesized that the CS in our blended graft could act as a sacrificial material and would promote better cellular infiltration, vascular neotissue formation, and overcome the high density (small pore size) of traditional electrospun nanofibers made of only one polymer type. We believe that fast degradation of our CS blended scaffold led to well-organized endothelialization, SMC differentiation and proliferation, and ECM deposition. Zhou *et al.* reported that an electrospun PCL/CS nanofiber TEVG seeded with ECs demonstrated endothelialization, elastin and collagen deposition without intimal hyperplasia at 3 months in a dog model [18], thus supporting our current results.

In 1999, a porous CS-based scaffold was introduced and seeded with human coronary artery endothelial cells and smooth muscle cells. The CS scaffold demonstrated favorable cellular adhesion and promoted vascular cell proliferation [35, 36]. The possible advantages of utilizing CS for tissue engineering applications include its low cost, large-scale availability, anti-microbial properties, and biocompatibility [37]. Furthermore, CS is cationic, degrades rapidly, and shares many structural similarities to naturally occurring glycosaminoglycans (GAGs) [38]. The cationic nature of CS is hypothetically beneficial because of its ability to interact with anionic GAGs, heparin, proteoglycans, and DNA or RNA nucleotides, and other molecules. This characteristic could benefit the development of CS scaffolds with conjugated cytokines,

growth factors, and other therapeutics such as transforming growth factor-beta (TGF- β) and platelet-derived growth factor (PDGF). The rapid degradation characteristic of CS are mainly attributed *in vivo* to lysozymal processing by macrophage and foreign body giant cells which leads to hydrolysis of acetylated residues and formation of non-toxic oligosaccharides, which can be incorporated in metabolic pathways or excreted [39, 40]. Moreover, the degradation rate of CS is highly dependent on its molecular weight and degree of deacetylation, parameters which could be manipulated to create an optimized tissue engineering scaffold with a rationally designed degradation profile [40, 41].

Our *in vitro* and *in vivo* results demonstrated the fast degradation and adequate mechanical properties of electrospun PCL/CS nanofiber TEVGs. The *in vitro* degradation results demonstrated a 50% decrease in ultimate tensile strength (UTS) within 2 weeks. In contrast, PCL by itself remains stable for many months *in vitro* [42]. The lack of mass loss suggests that rather than the scaffold degrading, chitosan aids the rapid loss of mechanical integrity by creating breaks in the PCL nanofibers. In addition to displaying adequate mechanical strength at 6 months, the TEVG burst pressure was comparable to that of native CA, and the compliance was about half of native CA. TEVGs abundant with ECM and collagen may lead to burst pressures comparable to that of native CA. However, TEVGs with less elastin and SMC volumes than that of native CA may lead to low compliance. Nonetheless, PCL/CS TEVG compliance may closely match that of native CA once long-term remodeling is completed.

Furthermore, the TEVGs in the current study displayed very small amounts of remaining scaffold material (remaining area average $9.12 \pm 5.41\%$) and no calcification. In contrast to our result, plain PCL scaffolds in a rat aortic interposition model developed chronic vascular calcification [19]. Vascular SMCs express transcription factors of both osteogenesis and osteoclastogenesis, can undergo osteogenic differentiation and calcification, and potentially prevent calcium deposition [43, 44]. Our previous study demonstrated that when compared to small-pore ($0.7\mu\text{m}$) nanofiber TEVGs, large-pore ($30\mu\text{m}$) TEVGs had abundantly more SMCs, displayed well-organized neointima, and better prevented calcific deposition [13]. Our results indicate that blended PCL/CS nanofiber TEVGs sufficiently formed vascular neotissue without calcification, but there is still a need for longer-term studies to evaluate these scaffolds until complete polymer degradation before clinical application can be advocated.

Several studies have investigated the patency rates of small diameter TEVGs implanted as CA conduits in large animal models [16–18, 45, 46]. We demonstrated that our blended PCL/CS (20:1 weight ratio) nanofiber TEVG was patent in 4 out of 6 cases (66.7%) using a postoperative course of aspirin. Another group with identical implantation and postoperative care methods investigated a PCL/CS nanofiber (1:1 weight ratio) TEVG with EC seeding. 5 out of 6 cases (83.3%) were patent at 3 months, however only 1 out of 6 control TEVGs without outgrowth EC seeding were patent, and the occluded cases were due to thrombosis within 2 months [18]. We suggest that these outcomes are due to the cationic nature of CS that leads to poor hemocompatibility due to undesirable adhesion with anionic platelets [25]. Therefore, the PCL to CS ratio becomes a more important factor for unseeded TEVG applications *in vivo* because the immediate risk of thrombosis must be weighed against the degradation rate and scaffold pore size (among other variables) to create the optimal cell-free construct [18, 25, 31].

With regards to long-term vascular remodeling, we found a significant positive correlation between TEVG wall thickness and CD68⁺ macrophage infiltration into the scaffold ($R^2 = 0.95$, $p = 0.0010$). Our previous studies suggested that excessive macrophage infiltration contributes to vascular neotissue hyperplasia, which leads to stenosis and graft occlusion [47, 48]. However, acute thrombosis cannot be ruled out in this study as a cause of graft occlusion because ultrasound revealed that both stenotic TEVGs were occluded by 1-month follow-up. It is difficult to ascertain whether the cause of stenosis/occlusion in our 6-month study is due to acute

thrombosis, neointimal hyperplasia, or a combination of both processes. Even though cell seeding improves TEVG patency, including such a process diminishes a scaffold's "off-the-shelf" potential and greatly increases the regulatory burden required to bring the product to market.

Vascular SMCs can perform both contractile and synthetic functions [49], and thus have the necessary flexibility to efficiently assume a spectrum of phenotypes under different physiological and pathological conditions. SMCs are characterized by changes in morphology, proliferation and migration rates, and the expression of different marker proteins [49, 50]. Immunohistochemistry of the PCL/CS scaffold encouragingly demonstrated the completion of SMC differentiation and migration *in vivo* at 6 months. In the TEVG, a circumferentially aligned multilayer of contractile SMCs was similar in thickness and density to that found in the native CA. However upon searching the literature, there were no representative staining images of vascular SMC maturation in biodegradable vascular scaffolds in a sheep model. For the first time, we show that CS's fast degrading properties encourages transanastomotic [51] or transmural [52] migration of synthetic SMCs and their differentiation and maturation in a sheep CA model.

Limitations

While the results of this study are promising and clearly encourage further investigation, this experiment was limited by the short length of the scaffolds and small number of animals in the study. Large animal studies investigating small-diameter TEVG longer than 5cm in length indicate low patency at the intermediate follow-up time point [18, 53]. Furthermore, though patency rates are better during short-term follow-up, it is difficult to evaluate neotissue formation due to the amount of scaffold remaining at these time points. We used short length TEVGs (1.5cm) in a large animal model to maintain graft patency and explanted them at 6 months to evaluate vascular neotissue formation. Future studies should investigate the degree of neotissue formation at extended follow-up time points after complete scaffold degradation. In addition, cell-free TEVGs longer than 5cm should be implanted and evaluated for graft patency and remodeling before initiation of human clinical trials. Despite our study limitations, the cell-free electrospun PCL/CS nanofiber TEVGs investigated in this report provided important information regarding vascular remodeling, occlusive complications and the degree of neotissue formation at the 6-month time point.

Conclusions

Unseeded electrospun blended PCL/CS nanofiber TEVGs might be an attractive alternative to small diameter prosthetic vascular grafts for the management of coronary artery and peripheral vascular disease. The fast degradation profile leads to rapid cellular infiltration, improved vascular remodeling, and neotissue formation without calcification or aneurysm. We are the first to demonstrate vascular SMC maturation in an electrospun biodegradable scaffold in the sheep model. Despite study limitations, such as graft length and time course, our novel hybrid PCL/CS TEVG warrants further investigation due to its great clinical potential and "off-the-shelf" availability.

Acknowledgments

This study was supported by grants from the NIH Center for Accelerated Innovations: Technology Development Program (1UH54HL119810-01) and by electrospun nanofiber PCL/CS Tissue Engineered Vascular Grafts from Nanofiber Solution Inc. C.Breuer and T.Shinoka received grant support from Gunze Ltd (Kyoto, Japan).

Author Contributions

Conceived and designed the experiments: TF T. Shinoka C. Breuer JJ NH. Performed the experiments: TF C. Best T. Sugiura T. Shoji TY BU DO NH. Analyzed the data: TF C. Best DO JJ. Contributed reagents/materials/analysis tools: TF C. Best T. Sugiura TY T. Shinoka C. Breuer BU DO JJ NH. Wrote the paper: TF C. Best T. Shoji T. Shinoka C. Breuer JJ CSO HZ NH. Mouse study: TY T. Shinoka C. Breuer BU DO JJ NH. Sheep study: TF C. Best T. Sugiura T. Shoji T. Shinoka C. Breuer DO JJ NH.

References

1. Stehouwer CD, Clement D, Davidson C, Diehm C, Elte JW, Lambert M, et al. Peripheral arterial disease: a growing problem for the internist. *Eur J Intern Med.* 2009; 20(2):132–8. doi: [10.1016/j.ejim.2008.09.013](https://doi.org/10.1016/j.ejim.2008.09.013) PMID: [19327600](https://pubmed.ncbi.nlm.nih.gov/19327600/).
2. Ravi S, Chaikof EL. Biomaterials for vascular tissue engineering. *Regen Med.* 2010; 5(1):107–20. doi: [10.2217/rme.09.77](https://doi.org/10.2217/rme.09.77) PMID: [20017698](https://pubmed.ncbi.nlm.nih.gov/20017698/); PubMed Central PMCID: [PMCPMC2822541](https://pubmed.ncbi.nlm.nih.gov/pmc/articles/PMC2822541/).
3. Dorigo W, Pulli R, Castelli P, Dorrucchi V, Ferilli F, De Blasis G, et al. A multicenter comparison between autologous saphenous vein and heparin-bonded expanded polytetrafluoroethylene (ePTFE) graft in the treatment of critical limb ischemia in diabetics. *J Vasc Surg.* 2011; 54(5):1332–8. doi: [10.1016/j.jvs.2011.05.046](https://doi.org/10.1016/j.jvs.2011.05.046) PMID: [21840151](https://pubmed.ncbi.nlm.nih.gov/21840151/).
4. Lindholt JS, Gottschalksen B, Johannesen N, Dueholm D, Ravn H, Christensen ED, et al. The Scandinavian Propaten((R)) trial—1-year patency of PTFE vascular prostheses with heparin-bonded luminal surfaces compared to ordinary pure PTFE vascular prostheses—a randomised clinical controlled multi-centre trial. *Eur J Vasc Endovasc Surg.* 2011; 41(5):668–73. doi: [10.1016/j.ejvs.2011.01.021](https://doi.org/10.1016/j.ejvs.2011.01.021) PMID: [21376643](https://pubmed.ncbi.nlm.nih.gov/21376643/).
5. Pulli R, Dorigo W, Castelli P, Dorrucchi V, Ferilli F, De Blasis G, et al. Midterm results from a multicenter registry on the treatment of infrainguinal critical limb ischemia using a heparin-bonded ePTFE graft. *J Vasc Surg.* 2010; 51(5):1167–77 e1. doi: [10.1016/j.jvs.2009.12.042](https://doi.org/10.1016/j.jvs.2009.12.042) PMID: [20347549](https://pubmed.ncbi.nlm.nih.gov/20347549/).
6. Zheng W, Wang Z, Song L, Zhao Q, Zhang J, Li D, et al. Endothelialization and patency of RGD-functionalized vascular grafts in a rabbit carotid artery model. *Biomaterials.* 2012; 33(10):2880–91. doi: [10.1016/j.biomaterials.2011.12.047](https://doi.org/10.1016/j.biomaterials.2011.12.047) PMID: [22244694](https://pubmed.ncbi.nlm.nih.gov/22244694/).
7. Roh JD, Sawh-Martinez R, Brennan MP, Jay SM, Devine L, Rao DA, et al. Tissue-engineered vascular grafts transform into mature blood vessels via an inflammation-mediated process of vascular remodeling. *Proc Natl Acad Sci U S A.* 2010; 107(10):4669–74. doi: [10.1073/pnas.0911465107](https://doi.org/10.1073/pnas.0911465107) PMID: [20207947](https://pubmed.ncbi.nlm.nih.gov/20207947/); PubMed Central PMCID: [PMCPMC2842056](https://pubmed.ncbi.nlm.nih.gov/pmc/articles/PMC2842056/).
8. Chung S, Ingle NP, Montero GA, Kim SH, King MW. Bioresorbable elastomeric vascular tissue engineering scaffolds via melt spinning and electrospinning. *Acta Biomater.* 2010; 6(6):1958–67. doi: [10.1016/j.actbio.2009.12.007](https://doi.org/10.1016/j.actbio.2009.12.007) PMID: [20004258](https://pubmed.ncbi.nlm.nih.gov/20004258/).
9. Hong Y, Ye SH, Nieponice A, Soletti L, Vorp DA, Wagner WR. A small diameter, fibrous vascular conduit generated from a poly(ester urethane)urea and phospholipid polymer blend. *Biomaterials.* 2009; 30(13):2457–67. doi: [10.1016/j.biomaterials.2009.01.013](https://doi.org/10.1016/j.biomaterials.2009.01.013) PMID: [19181378](https://pubmed.ncbi.nlm.nih.gov/19181378/); PubMed Central PMCID: [PMCPMC2698791](https://pubmed.ncbi.nlm.nih.gov/pmc/articles/PMC2698791/).
10. Lovett ML, Cannizzaro CM, Vunjak-Novakovic G, Kaplan DL. Gel spinning of silk tubes for tissue engineering. *Biomaterials.* 2008; 29(35):4650–7. doi: [10.1016/j.biomaterials.2008.08.025](https://doi.org/10.1016/j.biomaterials.2008.08.025) PMID: [18801570](https://pubmed.ncbi.nlm.nih.gov/18801570/); PubMed Central PMCID: [PMCPMC3206260](https://pubmed.ncbi.nlm.nih.gov/pmc/articles/PMC3206260/).
11. Sarkar S, Sales KM, Hamilton G, Seifalian AM. Addressing thrombogenicity in vascular graft construction. *J Biomed Mater Res B Appl Biomater.* 2007; 82(1):100–8. doi: [10.1002/jbm.b.30710](https://doi.org/10.1002/jbm.b.30710) PMID: [17078085](https://pubmed.ncbi.nlm.nih.gov/17078085/).
12. L'Heureux N, Dusserre N, Konig G, Victor B, Keire P, Wight TN, et al. Human tissue-engineered blood vessels for adult arterial revascularization. *Nat Med.* 2006; 12(3):361–5. doi: [10.1038/nm1364](https://doi.org/10.1038/nm1364) PMID: [16491087](https://pubmed.ncbi.nlm.nih.gov/16491087/); PubMed Central PMCID: [PMCPMC1513140](https://pubmed.ncbi.nlm.nih.gov/pmc/articles/PMC1513140/).
13. Tara S, Kurobe H, Rocco KA, Maxfield MW, Best CA, Yi T, et al. Well-organized neointima of large-pore poly(L-lactic acid) vascular graft coated with poly(L-lactic-co-epsilon-caprolactone) prevents calcific deposition compared to small-pore electrospun poly(L-lactic acid) graft in a mouse aortic implantation model. *Atherosclerosis.* 2014; 237(2):684–91. doi: [10.1016/j.atherosclerosis.2014.09.030](https://doi.org/10.1016/j.atherosclerosis.2014.09.030) PMID: [25463106](https://pubmed.ncbi.nlm.nih.gov/25463106/); PubMed Central PMCID: [PMCPMC4262639](https://pubmed.ncbi.nlm.nih.gov/pmc/articles/PMC4262639/).
14. Tara S, Rocco KA, Hibino N, Sugiura T, Kurobe H, Breuer CK, et al. Vessel bioengineering. *Circ J.* 2014; 78(1):12–9. PMID: [24334558](https://pubmed.ncbi.nlm.nih.gov/24334558/).

15. Mahara A, Somekawa S, Kobayashi N, Hirano Y, Kimura Y, Fujisato T, et al. Tissue-engineered acellular small diameter long-bypass grafts with neointima-inducing activity. *Biomaterials*. 2015; 58:54–62. doi: [10.1016/j.biomaterials.2015.04.031](https://doi.org/10.1016/j.biomaterials.2015.04.031) PMID: [25941782](https://pubmed.ncbi.nlm.nih.gov/25941782/).
16. Row S, Peng H, Schlaich EM, Koenigsnecht C, Andreadis ST, Swartz DD. Arterial grafts exhibiting unprecedented cellular infiltration and remodeling in vivo: the role of cells in the vascular wall. *Biomaterials*. 2015; 50:115–26. doi: [10.1016/j.biomaterials.2015.01.045](https://doi.org/10.1016/j.biomaterials.2015.01.045) PMID: [25736502](https://pubmed.ncbi.nlm.nih.gov/25736502/); PubMed Central PMCID: [PMC4350022](https://pubmed.ncbi.nlm.nih.gov/PMC4350022/).
17. Mrowczynski W, Mugnai D, de Valence S, Tille JC, Khabiri E, Cikirikcioglu M, et al. Porcine carotid artery replacement with biodegradable electrospun poly-ε-caprolactone vascular prosthesis. *J Vasc Surg*. 2014; 59(1):210–9. doi: [10.1016/j.jvs.2013.03.004](https://doi.org/10.1016/j.jvs.2013.03.004) PMID: [23707057](https://pubmed.ncbi.nlm.nih.gov/23707057/).
18. Zhou M, Qiao W, Liu Z, Shang T, Qiao T, Mao C, et al. Development and in vivo evaluation of small-diameter vascular grafts engineered by outgrowth endothelial cells and electrospun chitosan/poly(ε-caprolactone) nanofibrous scaffolds. *Tissue Eng Part A*. 2014; 20(1–2):79–91. doi: [10.1089/ten.tea.2013.0020](https://doi.org/10.1089/ten.tea.2013.0020) PMID: [23902162](https://pubmed.ncbi.nlm.nih.gov/23902162/); PubMed Central PMCID: [PMC3875210](https://pubmed.ncbi.nlm.nih.gov/PMC3875210/).
19. de Valence S, Tille JC, Mugnai D, Mrowczynski W, Gurny R, Moller M, et al. Long term performance of polycaprolactone vascular grafts in a rat abdominal aorta replacement model. *Biomaterials*. 2012; 33(1):38–47. doi: [10.1016/j.biomaterials.2011.09.024](https://doi.org/10.1016/j.biomaterials.2011.09.024) PMID: [21940044](https://pubmed.ncbi.nlm.nih.gov/21940044/).
20. Kurobe H, Maxfield MW, Tara S, Rocco KA, Bagi PS, Yi T, et al. Development of small diameter nanofiber tissue engineered arterial grafts. *PLoS One*. 2015; 10(4):e0120328. doi: [10.1371/journal.pone.0120328](https://doi.org/10.1371/journal.pone.0120328) PMID: [25830942](https://pubmed.ncbi.nlm.nih.gov/25830942/); PubMed Central PMCID: [PMC4382213](https://pubmed.ncbi.nlm.nih.gov/PMC4382213/).
21. Chen ZG, Wang PW, Wei B, Mo XM, Cui FZ. Electrospun collagen-chitosan nanofiber: a biomimetic extracellular matrix for endothelial cell and smooth muscle cell. *Acta Biomater*. 2010; 6(2):372–82. doi: [10.1016/j.actbio.2009.07.024](https://doi.org/10.1016/j.actbio.2009.07.024) PMID: [19632361](https://pubmed.ncbi.nlm.nih.gov/19632361/).
22. Feng ZQ, Chu X, Huang NP, Wang T, Wang Y, Shi X, et al. The effect of nanofibrous galactosylated chitosan scaffolds on the formation of rat primary hepatocyte aggregates and the maintenance of liver function. *Biomaterials*. 2009; 30(14):2753–63. doi: [10.1016/j.biomaterials.2009.01.053](https://doi.org/10.1016/j.biomaterials.2009.01.053) PMID: [19232710](https://pubmed.ncbi.nlm.nih.gov/19232710/).
23. Garg K, Sell SA, Madurantakam P, Bowlin GL. Angiogenic potential of human macrophages on electrospun bioresorbable vascular grafts. *Biomed Mater*. 2009; 4(3):031001. doi: [10.1088/1748-6041/4/3/031001](https://doi.org/10.1088/1748-6041/4/3/031001) PMID: [19372619](https://pubmed.ncbi.nlm.nih.gov/19372619/).
24. Prabhakaran MP, Venugopal JR, Chyan TT, Hai LB, Chan CK, Lim AY, et al. Electrospun biocomposite nanofibrous scaffolds for neural tissue engineering. *Tissue Eng Part A*. 2008; 14(11):1787–97. doi: [10.1089/ten.tea.2007.0393](https://doi.org/10.1089/ten.tea.2007.0393) PMID: [18657027](https://pubmed.ncbi.nlm.nih.gov/18657027/).
25. Yao Y, Wang J, Cui Y, Xu R, Wang Z, Zhang J, et al. Effect of sustained heparin release from PCL/chitosan hybrid small-diameter vascular grafts on anti-thrombogenic property and endothelialization. *Acta Biomater*. 2014; 10(6):2739–49. doi: [10.1016/j.actbio.2014.02.042](https://doi.org/10.1016/j.actbio.2014.02.042) PMID: [24602806](https://pubmed.ncbi.nlm.nih.gov/24602806/).
26. Johnson J, Ohst D, Groehl T, Hettterscheidt, Jones M. Development of Novel, Bioresorbable, Small-Diameter Electrospun Vascular Grafts. *J Tissue Sci Eng*. 2015; 6:151. doi: [10.4172/2157-7552.1000151](https://doi.org/10.4172/2157-7552.1000151)
27. Bergmeister H, Schreiber C, Grasl C, Walter I, Plasenzotti R, Stoiber M, et al. Healing characteristics of electrospun polyurethane grafts with various porosities. *Acta Biomater*. 2013; 9(4):6032–40. doi: [10.1016/j.actbio.2012.12.009](https://doi.org/10.1016/j.actbio.2012.12.009) PMID: [23237988](https://pubmed.ncbi.nlm.nih.gov/23237988/).
28. Raghavan ML, Vorp DA. Toward a biomechanical tool to evaluate rupture potential of abdominal aortic aneurysm: identification of a finite strain constitutive model and evaluation of its applicability. *J Biomech*. 2000; 33(4):475–82. PMID: [10768396](https://pubmed.ncbi.nlm.nih.gov/10768396/).
29. Vorp DA, Schiro BJ, Ehrlich MP, Juvonen TS, Ergin MA, Griffith BP. Effect of aneurysm on the tensile strength and biomechanical behavior of the ascending thoracic aorta. *Ann Thorac Surg*. 2003; 75(4):1210–4. PMID: [12683565](https://pubmed.ncbi.nlm.nih.gov/12683565/).
30. Roh JD, Nelson GN, Brennan MP, Mirensky TL, Yi T, Hazlett TF, et al. Small-diameter biodegradable scaffolds for functional vascular tissue engineering in the mouse model. *Biomaterials*. 2008; 29(10):1454–63. doi: [10.1016/j.biomaterials.2007.11.041](https://doi.org/10.1016/j.biomaterials.2007.11.041) PMID: [18164056](https://pubmed.ncbi.nlm.nih.gov/18164056/); PubMed Central PMCID: [PMC2375856](https://pubmed.ncbi.nlm.nih.gov/PMC2375856/).
31. Sarasam A, Madihally SV. Characterization of chitosan-polycaprolactone blends for tissue engineering applications. *Biomaterials*. 2005; 26(27):5500–8. doi: [10.1016/j.biomaterials.2005.01.071](https://doi.org/10.1016/j.biomaterials.2005.01.071) PMID: [15860206](https://pubmed.ncbi.nlm.nih.gov/15860206/).
32. Du F, Wang H, Zhao W, Li D, Kong D, Yang J, et al. Gradient nanofibrous chitosan/poly(varepsilon-caprolactone) scaffolds as extracellular microenvironments for vascular tissue engineering. *Biomaterials*. 2012; 33(3):762–70. doi: [10.1016/j.biomaterials.2011.10.037](https://doi.org/10.1016/j.biomaterials.2011.10.037) PMID: [22056285](https://pubmed.ncbi.nlm.nih.gov/22056285/).
33. Zhang H, Neau SH. In vitro degradation of chitosan by a commercial enzyme preparation: effect of molecular weight and degree of deacetylation. *Biomaterials*. 2001; 22(12):1653–8. PMID: [11374467](https://pubmed.ncbi.nlm.nih.gov/11374467/).

34. Yang YM, Hu W, Wang XD, Gu XS. The controlling biodegradation of chitosan fibers by N-acetylation in vitro and in vivo. *J Mater Sci Mater Med*. 2007; 18(11):2117–21. doi: [10.1007/s10856-007-3013-x](https://doi.org/10.1007/s10856-007-3013-x) PMID: [17619982](https://pubmed.ncbi.nlm.nih.gov/17619982/).
35. Madhally SV, Matthew HW. Porous chitosan scaffolds for tissue engineering. *Biomaterials*. 1999; 20(12):1133–42. PMID: [10382829](https://pubmed.ncbi.nlm.nih.gov/10382829/).
36. Chupa JM, Foster AM, Sumner SR, Madhally SV, Matthew HW. Vascular cell responses to polysaccharide materials: in vitro and in vivo evaluations. *Biomaterials*. 2000; 21(22):2315–22. PMID: [11026638](https://pubmed.ncbi.nlm.nih.gov/11026638/).
37. Huang Y, Onyeri S, Siewe M, Moshfeghian A, Madhally SV. In vitro characterization of chitosan-gelatin scaffolds for tissue engineering. *Biomaterials*. 2005; 26(36):7616–27. doi: [10.1016/j.biomaterials.2005.05.036](https://doi.org/10.1016/j.biomaterials.2005.05.036) PMID: [16005510](https://pubmed.ncbi.nlm.nih.gov/16005510/).
38. Drury JL, Mooney DJ. Hydrogels for tissue engineering: scaffold design variables and applications. *Biomaterials*. 2003; 24(24):4337–51. PMID: [12922147](https://pubmed.ncbi.nlm.nih.gov/12922147/).
39. Pangburn SH, Trescony PV, Heller J. Lysozyme degradation of partially deacetylated chitin, its films and hydrogels. *Biomaterials*. 1982; 3(2):105–8. PMID: [7082736](https://pubmed.ncbi.nlm.nih.gov/7082736/).
40. Hirano S, Tsuchida H, Nagao N. N-acetylation in chitosan and the rate of its enzymic hydrolysis. *Biomaterials*. 1989; 10(8):574–6. PMID: [2605289](https://pubmed.ncbi.nlm.nih.gov/2605289/).
41. VandeVord PJ, Matthew HW, DeSilva SP, Mayton L, Wu B, Wooley PH. Evaluation of the biocompatibility of a chitosan scaffold in mice. *J Biomed Mater Res*. 2002; 59(3):585–90. PMID: [11774317](https://pubmed.ncbi.nlm.nih.gov/11774317/).
42. Johnson J, Niehaus A, Nichols S, Lee D, Koepsel J, Anderson D, et al. Electrospun PCL in vitro: a microstructural basis for mechanical property changes. *J Biomater Sci Polym Ed*. 2009; 20(4):467–81. doi: [10.1163/156856209X416485](https://doi.org/10.1163/156856209X416485) PMID: [19228448](https://pubmed.ncbi.nlm.nih.gov/19228448/).
43. Speer MY, Yang HY, Brabb T, Leaf E, Look A, Lin WL, et al. Smooth muscle cells give rise to osteochondrogenic precursors and chondrocytes in calcifying arteries. *Circ Res*. 2009; 104(6):733–41. doi: [10.1161/CIRCRESAHA.108.183053](https://doi.org/10.1161/CIRCRESAHA.108.183053) PMID: [19197075](https://pubmed.ncbi.nlm.nih.gov/19197075/); PubMed Central PMCID: [PMCPMC2716055](https://pubmed.ncbi.nlm.nih.gov/PMC/PMC2716055/).
44. Sun Y, Byon CH, Yuan K, Chen J, Mao X, Heath JM, et al. Smooth muscle cell-specific runx2 deficiency inhibits vascular calcification. *Circ Res*. 2012; 111(5):543–52. doi: [10.1161/CIRCRESAHA.112.267237](https://doi.org/10.1161/CIRCRESAHA.112.267237) PMID: [22773442](https://pubmed.ncbi.nlm.nih.gov/22773442/); PubMed Central PMCID: [PMCPMC3678289](https://pubmed.ncbi.nlm.nih.gov/PMC/PMC3678289/).
45. Koobatian MT, Row S, Smith RJ Jr., Koenigsnecht C, Andreadis ST, Swartz DD. Successful endothelialization and remodeling of a cell-free small-diameter arterial graft in a large animal model. *Biomaterials*. 2016; 76:344–58. doi: [10.1016/j.biomaterials.2015.10.020](https://doi.org/10.1016/j.biomaterials.2015.10.020) PMID: [26561932](https://pubmed.ncbi.nlm.nih.gov/26561932/); PubMed Central PMCID: [PMCPMC4662921](https://pubmed.ncbi.nlm.nih.gov/PMC/PMC4662921/).
46. Rothuizen TC, Damanik FF, Lavrijsen T, Visser MJ, Hamming JF, Lalai RA, et al. Development and evaluation of in vivo tissue engineered blood vessels in a porcine model. *Biomaterials*. 2016; 75:82–90. doi: [10.1016/j.biomaterials.2015.10.023](https://doi.org/10.1016/j.biomaterials.2015.10.023) PMID: [26491997](https://pubmed.ncbi.nlm.nih.gov/26491997/).
47. Hibino N, Yi T, Duncan DR, Rathore A, Dean E, Naito Y, et al. A critical role for macrophages in neovessel formation and the development of stenosis in tissue-engineered vascular grafts. *FASEB J*. 2011; 25(12):4253–63. doi: [10.1096/fj.11-186585](https://doi.org/10.1096/fj.11-186585) PMID: [21865316](https://pubmed.ncbi.nlm.nih.gov/21865316/); PubMed Central PMCID: [PMCPMC3236622](https://pubmed.ncbi.nlm.nih.gov/PMC/PMC3236622/).
48. Hibino N, Mejias D, Pietris N, Dean E, Yi T, Best C, et al. The innate immune system contributes to tissue-engineered vascular graft performance. *FASEB J*. 2015; 29(6):2431–8. doi: [10.1096/fj.14-268334](https://doi.org/10.1096/fj.14-268334) PMID: [25713026](https://pubmed.ncbi.nlm.nih.gov/25713026/); PubMed Central PMCID: [PMCPMC4447224](https://pubmed.ncbi.nlm.nih.gov/PMC/PMC4447224/).
49. Rensen SS, Doevendans PA, van Eys GJ. Regulation and characteristics of vascular smooth muscle cell phenotypic diversity. *Neth Heart J*. 2007; 15(3):100–8. PMID: [17612668](https://pubmed.ncbi.nlm.nih.gov/17612668/); PubMed Central PMCID: [PMCPMC1847757](https://pubmed.ncbi.nlm.nih.gov/PMC/PMC1847757/).
50. Owens GK. Regulation of differentiation of vascular smooth muscle cells. *Physiol Rev*. 1995; 75(3):487–517. PMID: [7624392](https://pubmed.ncbi.nlm.nih.gov/7624392/).
51. Hibino N, Villalona G, Pietris N, Duncan DR, Schoffner A, Roh JD, et al. Tissue-engineered vascular grafts form neovessels that arise from regeneration of the adjacent blood vessel. *FASEB J*. 2011; 25(8):2731–9. doi: [10.1096/fj.11-182246](https://doi.org/10.1096/fj.11-182246) PMID: [21566209](https://pubmed.ncbi.nlm.nih.gov/21566209/); PubMed Central PMCID: [PMCPMC3136337](https://pubmed.ncbi.nlm.nih.gov/PMC/PMC3136337/).
52. Clowes AW, Kirkman TR, Reidy MA. Mechanisms of arterial graft healing. Rapid transmural capillary ingrowth provides a source of intimal endothelium and smooth muscle in porous PTFE prostheses. *Am J Pathol*. 1986; 123(2):220–30. PMID: [3706490](https://pubmed.ncbi.nlm.nih.gov/3706490/); PubMed Central PMCID: [PMCPMC1888315](https://pubmed.ncbi.nlm.nih.gov/PMC/PMC1888315/).
53. Pashneh-Tala S, MacNeil S, Claeysens F. The Tissue-Engineered Vascular Graft—Past, Present, and Future. *Tissue Eng Part B Rev*. 2015. doi: [10.1089/ten.teb.2015.0100](https://doi.org/10.1089/ten.teb.2015.0100) PMID: [26447530](https://pubmed.ncbi.nlm.nih.gov/26447530/).